A NOVEL HYBRID ANT COLONY OPTIMIZATION AND PARTICLE SWARM OPTIMIZATION ALGORITHM FOR INVERSE PROBLEMS OF COUPLED RADIATIVE AND CONDUCTIVE HEAT TRANSFER

by

Biao ZHANG, Hong QI*, Shuang-Cheng SUN, Li-Ming RUAN*, and He-Ping TAN

School of Energy Science and Engineering, Harbin Institute of Technology, Harbin, China

Original scientific paper
DOI:10.2298/TSCI131124023Z

In this study, a continuous ant colony optimization algorithm on the basis of probability density function was applied to the inverse problems of 1-D coupled radiative and conductive heat transfer. To overcome the slow convergence of the ant colony optimization algorithm for continuous domain problems, a novel hybrid ant colony optimization and particle swarm optimization algorithm was proposed. To illustrate the performances of these algorithms, the thermal conductivity, absorption coefficient, and scattering coefficient of the 1-D homogeneous semi-transparent medium were retrieved for several test cases. The temperature and radiative heat flux simulated by the finite volume method were served as inputs for the inverse analysis. Through function estimation and parameter estimation, the hybrid colony and particle swarm optimization algorithm was proved to be effective and robust.

Key words: *inverse problem, ant colony optimization, particle swarm optimization, coupled heat transfer*

Introduction

Coupled radiative and conductive heat transfer in absorbing-emitting-scattering materials is pervasive in engineering applications, such as ceramic component for high-temperature use, tempering of glass windows, and insulating techniques for the protection of aero-engines [1]. If only considering the radiation or conduction in thermal analysis of these issues, it will produce an obvious deviation [2]. In the last two decades, considerable attention has been paid to the development of accurate and efficient methods for handling coupled radiative and conductive heat transfer [3-6].

Recently, due to the wide applications of coupled radiation and conduction, the inverse problems of them have drawn much attention all over the world [7-10]. A wide variety of solution techniques have been successfully employed in the inverse analyses of heat transfer, which can be roughly divided into two categories. One is the traditional algorithm based on gradient, and the other is the intelligent optimization algorithm [11]. Compared with traditional gradient-based methods, the intelligent optimization algorithms have the following outstanding characteristics: (1) both ill and non-linear inverse problems could be solved, (2) the inverse problems with complicated or no analytic expression could be solved, (3) the derivative of the objective function is not necessary, and (4) the priori information is not needed [12].

* Corresponding authors'; e-mails: qihong@hit.edu.cn, ruanlm@hit.edu.cn

The ant colony optimization (ACO) algorithm is a potential heuristic bionic evolutionary algorithm. It was proposed by Colorni *et al.* [13] in the early 1990s. The development of this algorithm was inspired by the ants' foraging behavior. It was first formalized by Dorigo *et al.* [14]. After more than ten years of development, the ACO algorithm has drawn the global attention, and its application fields have been rapidly expanded. Numerous studies show that ACO algorithm has positive feedback, parallelism, and robustness [15]. There are several types of ACO algorithms that can be used for continuous domain optimization problems. The probability density function (PDF) based ACO algorithm is one of the most efficient. The logical adaption would be to shift from the discrete probability distribution to a continuous PDF [16].

Although the ACO algorithm has many outstanding characteristics, it has its own defects. One of the most obvious drawbacks is that the convergence speed is too slow especially in the later stage. Many scholars focus on improving the performance of the ACO algorithm [17-19]. Particle swarm optimization (PSO) algorithm is one of the famous intelligent optimization algorithms, which has been successfully applied to continuous domain optimization [20-24]. Inspired by the PSO algorithm, a novel hybrid ACO and PSO (HAPO) algorithm is proposed based on the ACO algorithm.

In this paper, the novel HAPO algorithm is applied to solve the inverse problems of coupled radiative and conductive heat transfer. A 1-D homogenous participating gray slab medium is investigated. Several test cases are designed, where the thermal conductivity, absorption coefficient and scattering coefficient are retrieved by measuring the steady-state temperature and radiative flux on the borders. Through function estimation, parameter estimation and measurement error analysis, the HAPO algorithm is proved to be effective and robust.

Theories and methods

Forward model

Let us consider the steady-state coupled radiative and conductive heat transfer in an absorbing, emitting, and isotropic scattering plane-parallel slab with thickness L as shown in fig. 1 [7]. The refractive indices of the slab and the surroundings are both uniform and equal to 1.0. The boundaries of the slab are opaque diffuse gray. The emissivity of the left wall ($x = 0$) and the right wall ($x = L$) are given as ε_{w1} and ε_{w2}, respectively. The left wall is subjected to a convection boundary condition with the ambient temperature, T_{f1}, and convective heat transfer coefficient, h_{f1}. The right wall is also subjected to a convection boundary condition but with the ambient temperature, T_{f2}, and convective heat transfer coefficient, h_{f2}. The thermal conductivity, λ, absorption coefficient, κ_a, and scattering coefficient, κ_s, are supposed to be uniform and do not change over time.

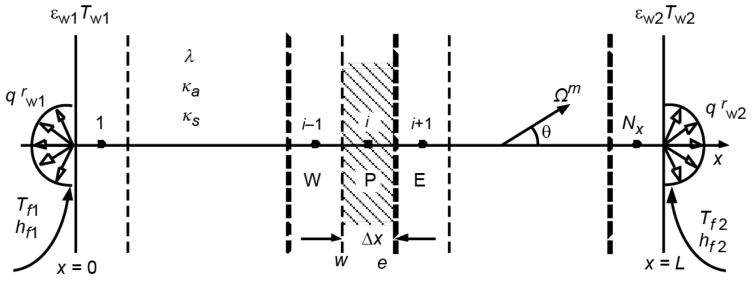

Figure 1. The schematic of coupled radiative and conductive heat transfer [7]

The 1-D energy conservation equation governing the steady-state coupled radiative and conductive heat transfer with constant physical parameters is defined:

$$\lambda \frac{\partial^2 T}{\partial x^2} = \nabla \vec{q}^{\,r} \tag{1}$$

where T is the medium temperature, $\nabla \vec{q}^{\,r}$ – the divergence of the radiative heat flux. It is given by:

$$\nabla \vec{q}^{\,r} = \kappa_a \left[4\pi I_b - \int_{4\pi} I \, d\Omega \right] \tag{2}$$

where $I_b = \sigma T^4/\pi$ is the blackbody radiation intensity, σ – the Stefan-Boltzmann constant, I – the radiation intensity at direction $\vec{\Omega}$, and Ω – the solid angle.

The convection boundary conditions are expressed:

$$q_{w1}^r - \lambda \left. \frac{\partial T}{\partial x} \right|_{x=0} = h_{f1}(T_{f1} - T_{w1}) \tag{3}$$

$$q_{w2}^r + \lambda \left. \frac{\partial T}{\partial x} \right|_{x=L} = h_{f2}(T_{f2} - T_{w2}) \tag{4}$$

where T_{w1} and T_{w2} are the temperatures of the left and right wall, respectively, q_{w1}^r and q_{w2}^r – the radiative heat fluxes on the left and right wall, respectively. They are defined:

$$q_{w1}^r = \varepsilon_{w1} \left[\sigma T_{w1}^4 - \int_{\vec{n}_{w1} \cdot \vec{\Omega} > 0} I \left| \vec{n}_{w1} \, \vec{\Omega} \right| d\Omega \right] \tag{5}$$

$$q_{w2}^r = \varepsilon_{w2} \left[\sigma T_{w2}^4 - \int_{\vec{n}_{w2} \cdot \vec{\Omega} > 0} I \left| \vec{n}_{w2} \, \vec{\Omega} \right| d\Omega \right] \tag{6}$$

where $\vec{\Omega}$ is the radiative direction, $\vec{n}_{w1}$ and $\vec{n}_{w2}$ are the outer normal directions of the left and right wall.

The radiative intensity I in eqs. (2), (5), and (6) can be calculated by radiative transfer equation (RTE) for absorbing-scattering-emitting gray slab medium, which is written:

$$\frac{dI(s, \vec{\Omega})}{ds} = -\kappa_e I(s, \vec{\Omega}) + \kappa_a I_b(s) + \frac{\kappa_s}{4\pi} \int_{\Omega'=4\pi} I(s, \vec{\Omega}) \, \Phi(\vec{\Omega}', \vec{\Omega}) \, d\Omega' \tag{7}$$

where ds is the length along the direction $\vec{\Omega}$, κ_e – the extinction coefficient, $I(s, \vec{\Omega})$ – the radiative intensity at position s and direction $\vec{\Omega}$, $\Phi(\vec{\Omega}', \vec{\Omega})$ – the scattering phase function between incoming direction $\vec{\Omega}'$, and scattering direction $\vec{\Omega}$.

The boundary conditions of opaque diffuse gray wall are expressed:

$$I_{w1}^+ = \varepsilon_{w1} I_{b,w1} + \frac{1 - \varepsilon_{w1}}{\pi} \int_{\vec{n}_{w1} \cdot \vec{\Omega} > 0} I_{w1} \left| \vec{n}_{w1} \, \vec{\Omega} \right| d\Omega \tag{8}$$

$$I_{w2}^- = \varepsilon_{w2} I_{b,w2} + \frac{1 - \varepsilon_{w2}}{\pi} \int_{\vec{n}_{w2} \cdot \vec{\Omega} > 0} I_{w2} \left| \vec{n}_{w2} \, \vec{\Omega} \right| d\Omega \tag{9}$$

where I_{w1}^+ and I_{w2}^- are the radiative intensities to the internal medium from left and right side of the wall, respectively, I_{w1} and I_{w2} – the radiative intensities in direction $\vec{\Omega}$ on the left

and right side of the wall, respectively, and $I_{b,w1}$ and $I_{b,w2}$ – the blackbody radiative intensities on the left and right side of the wall, respectively.

The energy equation and RTE can be simultaneously solved by finite volume method (FVM) for 1-D coupled radiative and conductive heat transfer model [25]. The temperature and the radiative intensity in each control solid angle can be calculated in each control volume. Furthermore, the temperatures and radiative heat fluxes on the borders can also be obtained.

Inverse model

Principle of PDF-based ACO algorithm

The original ACO algorithm is introduced to solve discrete optimization problems. However, the inverse problems of coupled radiative and conductive heat transfer are continuous domain optimization problems. The logical adaption would be also changing from using the discrete probability distribution to a continuous PDF. Instead of choosing a component at the i^{th} inversion parameter, the ants would generate a random number according to a certain PDF [16].

The number of the inversion parameters is assumed as N, and the amount of the dominant ant ranks is set as N_d. In each of N construction steps, an ant chooses a value x_i for exactly one of the dimensions. For performing this choice, an ant uses a Gaussian kernel, which is a weighted superposition of several Gaussian functions, as PDF. The probability density distribution of the i^{th} inversion parameter with the j^{th} rank at iteration t is expressed:

$$P_{i,j}(t) = w_{\tau_j} f_{\eta_{i,j}}(t) \tag{10}$$

where w_{τ_j} is the probability of selecting the j^{th} rank, which is determined by the pheromone value $\tau_j(t)$, $f_{\eta_{i,j}}(t)$ – the probability density distribution of a normal distribution with expectation $\mu_{i,j}(t)$ and standard deviation $\sigma_{i,j}(t)$.

The probability of selecting the j^{th} rank w_{τ_j} is defined:

$$w_{\tau_j} = \frac{\tau_j(t)}{\sum_{m=1}^{N_d} \tau_m(t)} \tag{11}$$

where $\tau_j(t)$ is the pheromone value of the j^{th} rank at iteration t. It can be defined:

$$\tau_j(t) = \frac{1}{\alpha N_d \sqrt{2\pi}} \exp\left[-\frac{(j-1)^2}{2\alpha^2 N_d^2} \right] \tag{12}$$

where α is a positive parameter which determines the relative importance of the rank.

The probability density distribution of a normal distribution $f_{\eta_{i,j}}(t)$ is defined:

$$f_{\eta_{i,j}}(t) = \frac{1}{\sqrt{2\pi}\sigma_{i,j}(t)} \exp\left\{ -\frac{\left[x_i - \mu_{i,j}(t) \right]^2}{2\sigma_{i,j}^2(t)} \right\} \tag{13}$$

where $\mu_{i,j}(t)$ is the retrieval value of the i^{th} inversion parameter with the j^{th} rank at iteration t, $\sigma_{i,j}(t)$ – the standard deviation of the i^{th} inversion parameter with the j^{th} rank at iteration t. It can be defined:

$$\sigma_{i,j}(t) = \beta \sqrt{\frac{1}{N_\mathrm{d}} \sum_{l=1}^{N_\mathrm{d}} \left[\mu_{i,l}(t) - \mu_{i,j}(t) \right]^2} \tag{14}$$

where β is a positive parameter which regulates the speed of convergence. The higher the value of β is, the lower the convergence speed of the algorithm will be.

Principle of HAPO algorithm

In PSO algorithm, each particle changes its position in the search space and updates its velocity according to its own flying experience and its neighbors' flying experience [20]. In a specific problem, one's flying experience denotes the local individual best location $P_{\mathrm{l},i}(t)$, and the neighbors' flying experience denotes the global best position $P_{\mathrm{g},i}(t)$. As shown in fig. 2, the algorithm updates the position $x_i(t+1)$ and the velocity $v_i(t+1)$ for each dimension of the i^{th} inversion parameter according to the following equations:

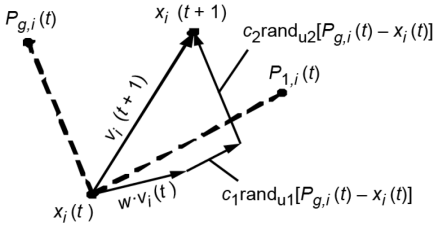

Figure 2. The schematic for bird foraging

$$x_i(t+1) = x_i(t) + v_i(t+1) \tag{15}$$

$$v_i(t+1) = w\, v_i(t) + c_1\ \mathrm{rand}_{u1}[P_{\mathrm{l},i}(t) - x_i(t)] + c_2\ \mathrm{rand}_{u2}[P_{\mathrm{g},i}(t) - x_i(t)] \tag{16}$$

where w is the inertia weight coefficient, which controls the impact of the previous velocity on the current velocity. The c_1 and c_2 are two positive constants called acceleration coefficient, rand_{u1} and rand_{u2} are two uniform random numbers in [0, 1].

In order to accelerate the convergence speed, the idea of the PSO algorithm is employed in updating the retrieval values of the i^{th} inversion parameter with rank 2 to N_d at iteration t.

$$\mu_{i,j}(t+1) = \mu_{i,j}(t) + \rho \left\{ c_1 \mathrm{rand}_{u1} \left[\mu_{i,1}(t) - \mu_{i,j}(t) \right] + c_2 \mathrm{rand}_{u2} \left[\mu_i(t) - \mu_{i,j}(t) \right] \right\} \tag{17}$$

$$\mu_i(t) = \frac{\sum_{j=1}^{N_\mathrm{d}} \mu_{i,j}(t)}{N_\mathrm{d}} \tag{18}$$

$$\rho = \max \frac{\xi}{F_{\mathrm{obj},1},\ 1} \tag{19}$$

where ρ is the positive parameter less than one, ξ – the small positive parameter, which determines the convergence speed.

Computation procedures of HAPO approaches

The procedure for implementing the HAPO algorithm is described as the following steps and the flowchart of the HAPO algorithm is shown in fig. 3.

Step 1. Input the size of the colony, N_a, the amount of the dominant ants, N_d, the number of the inversion parameters, N, the number of the measurement positions, N_m, the maximum of the iterations, N_g. Set the factor of pheromone value, α, the factor of heuristic information, β, the tolerance for minimizing the objective function, ε_o, the tolerance for minimizing the standard deviation, ε_d, the convergence speed control parameter, ξ, the acceleration coefficients, c_1 and c_2. Estimate the initial search space $[\text{low}_i, \text{high}_i]$ of each inversion parameter. Initialize the number of the iterations $t = 1$ and the probability density distribution, $P_{i,j}(t)$.

Step 2. Calculate the probability density distribution $P_{i,j}(t)$ of the i th inversion parameter with the j^{th} rank at iteration t using eq. (10). Solve the forward model based on the inversion parameter x_i using FVM. Furthermore, obtain the value of the objective function, F_{obj}. If the F_{obj} is smaller than the value of the N_d^{th} rank $F_{\text{obj},\,N_d}$, the corresponding retrieval value $\mu_{i,N_d}(t)$ will be replaced, and the retrieval value of each rank will be reordered according to the values of their objective functions.

Step 3. When all the ants finish constructing their solutions, update the retrieval value of each rank $\mu_{i,j}(t+1)$ using eq. (17). Furthermore, update the standard deviation $\sigma_{i,j}(t+1)$ of the i^{th} inversion parameter with the j^{th} rank using eq. (14). Then, set $t = t+1$ and complete one iteration.

Step 4. Loop to *Step 2* until the program satisfies one of the following three stop criterions:

(a) the value of objective function reaches the tolerance for minimizing the objective function ε_o, $F_{\text{obj}} < \varepsilon_o$;
(b) the maximum of the standard deviation meets the tolerance for minimizing the standard deviation ε_d, $\max\left\{\sigma_{i,j}(t)\right\} < \varepsilon_d$;
(c) the number of the iteration exceeds the maximum of the iterations N_g, $t > N_g$.

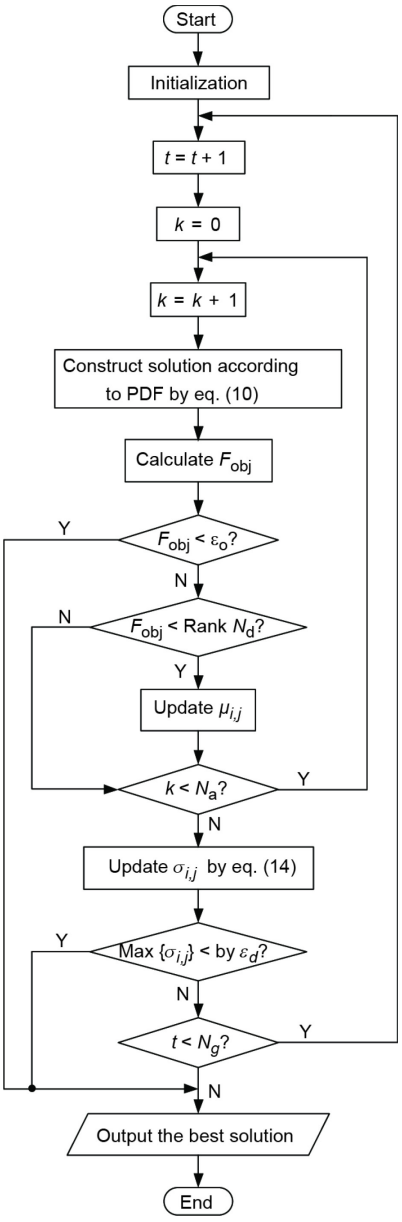

Figure 3. The flowchart of the HAPO

Results and discussions

Function estimation

To compare the performances of the ACO and HAPO algorithms, three famous benchmark optimization functions are used, which are described in tab. 1.

In the ACO algorithm, the system data and control parameters are set as $N_a = 30$, $N_d = 30$, $N_g = 1000$, $\alpha = 0.5$, $\beta = 1.5$, $\varepsilon_o = 10^{-8}$, and $\varepsilon_d = 10^{-4}$. Besides the same parameter values, we set the other parameters as $c_1 = 0.3$, $c_2 = 0.7$, and $\xi = 10^{-4}$ in HAPO algorithm.

Table 1. Details of the test functions

Function	Expression	Space	Required accuracy
Sphere	$f_1 = \sum_{i=1}^{N} x_i^2$	$[-100, 100]^N$	10^{-2}
Rosenbrock	$f_2 = \sum_{i=1}^{N-1} [100(x_{i+1} - x_i^2)^2 + (1 - x_i)^2]$	$[-30, 30]^N$	10^{-2}
Rastrigin	$f_3 = \sum_{i=1}^{N} [x_i^2 - 10\cos(2\pi x_i) + 10]$	$[-5.12, 5.12]^N$	10^{-2}

Table 2 shows the robustness analysis results for the proposed HAPO algorithm, in which the HAPO algorithm is implemented for 100 times. For comparison with the ACO algorithm, this paper has adopted two robustness measures, named succeed ratio and average valid evaluation number, which are given:

$$\mathrm{SR} = \frac{N_\mathrm{s}}{N_\mathrm{t}} 100 \tag{20}$$

$$\mathrm{AVEN} = \frac{\sum_{l=1}^{N_\mathrm{s}} t_l}{N_\mathrm{s}} \tag{21}$$

where N_s is the number of successes, which means the times of that the objective function reaches required accuracy in the N_t independent runs.

Table 2. Results of robustness analysis for the ACO and HAPO algorithms

Dim.	Sphere				Rosenbrock				Rastrigin			
	ACO		HAPO		ACO		HAPO		ACO		HAPO	
	SR [%]	AVEN	SR [%]	AVEN	SR [%]	AVEN	SR [%]	AVEN	SR [%]	AVEN	SR [%]	AVEN
1	100	8.48	100	6.47	–	–	–	–	100	11.31	100	10.79
2	100	20.28	100	16.41	100	163.48	100	98.29	100	55.48	100	46.04
3	100	36.65	100	27.49	99	911.04	98	491.03	90	235.04	78	258.65
4	100	62.67	100	45.92	96	1000.0	94	819.81	49	530.37	44	571.22
5	100	96.65	100	68.86	95	1000.0	97	1000.0	4	702.50	4	797.00
6	100	142.85	100	96.05	97	1000.0	98	1000.0	–	–	–	–
7	100	207.51	100	135.52	76	1000.0	66	993.36	–	–	–	–
8	100	290.92	100	187.19	1	1000.0	3	1000.0	–	–	–	–
9	100	405.79	100	253.05	–	–	–	–	–	–	–	–
10	100	558.26	100	331.78	–	–	–	–	–	–	–	–

From tab. 2, it can be observed that the results obtained by the ACO and HAPO algorithms are very close to theoretical optima when there is no local minimum, and the HAPO algorithm is superior to the ACO algorithm. When there are many local minimums, the performances of the two algorithms get deteriorate with the increasing of the dimensions.

Parameter estimation

To demonstrate the validity of the ACO algorithms in the inverse problems of coupled radiative and conductive heat transfer, two test cases of 1-D homogeneous semi-transparent gray slab medium model are investigated in the present study. The thermal conductivity, absorption coefficient, and scattering coefficient are retrieved to illustrate the performance of the ACO algorithms. The accuracies and efficiencies of the ACO and HAPO algorithms are compared.

Single parameter retrieval

In the model depicted in the chapter *Forward model*, the parameters are set:

L = 5 m, ε_{w1} = 0.9, ε_{w2} = 0.7, T_{f1} = 1000 K, h_{f1} = 20 W/m^{2}K, T_{f2} = 500 K, h_{f2} = = 10 W/m^{2}K. The thermal conductivity and scattering coefficient are known as λ = 20 W/mK and κ_s = 4.5 m^{-1}. The absorption coefficient κ_a is retrieved by measuring the temperature and radiative heat flux on the borders under the true absorption coefficients κ_a^* of 0.5, 1.5, 2.5, 3.5, and 4.5 m^{-1}. The measured values can be obtained by using the FVM approximation with N_x = 5000 and N_θ = 100.

The model validation and grids independence have been investigated in our previous work [7]. Finally, the FVM approximation with N_x = 300 and $N_x = 300$ and N_θ = 50 is used as the forward model in the inversion, and the objective function can be defined:

$$F_{obj} = \frac{1}{4}\left[(T_{w1} - T_{w1}^*)^2 + \frac{(q_{w1}^r - q_{w1}^{r*})^2}{10^4} + (T_{w2} - T_{w2}^*)^2 + \frac{(q_{w2}^r - q_{w2}^{r*})^2}{10^4} \right] \tag{22}$$

where T_{w1}, T_{w2}, q_{w1}^r, q_{w2}^r, and T_{w1}^*, T_{w2}^*, q_{w1}^{r*}, q_{w2}^{r*} represent the estimated and measured values, respectively.

Since the ACO-based algorithm is a stochastic optimization method, every optimization has certain randomness. The ACO and HAPO algorithms are repeated 100 times to reduce the effect of the randomness. The system data and control parameters are set: $N_a = 30$, $N_d = 5$, $N_g = 1000$, $\alpha = 0.5$, $\beta = 1.5$, $\varepsilon_o = 10^{-8}$, $c_1 = 0.3$, $c_2 = 0.7$, and $\xi = 10^{-4}$.

The retrieval results are shown in tab. 3, in which the initial search space of the absorption coefficient κ_a is $[1, 10]$. Because there is a linear relationship between iteration number and calculating time on the same computer configuration, while the iteration number is similar on different computer configurations, here we use the number of iterations instead of computation time. As shown in tab. 3, the efficiency of the HAPO algorithm is significantly higher than that of the ACO algorithm. However, the HAPO algorithm does not lose the

Table 3. The retrieval results of absorption coefficient using ACO and HAPO algorithms

No.	κ_a^* [m^{-1}]	ACO		HAPO	
		κ_a^* [m^{-1}]	Iteration, t	κ_a^* [m^{-1}]	Iteration, t
1	0.5	0.500±2.4·10^{-5}	6.1±0.98	0.500±4.1·10^{-5}	5.5±0.85
2	1.5	1.500±2.9·10^{-5}	6.0±1.11	1.500±4.8·10^{-5}	5.2±0.75
3	2.5	2.500±5.7·10^{-5}	5.4±0.98	2.500±5.3·10^{-5}	5.1±0.85
4	3.5	3.500±1.1·10^{-4}	5.0±0.97	3.500±1.1·10^{-4}	4.6±0.77
5	4.5	4.500±2.2·10^{-4}	4.6±0.89	4.500±2.3·10^{-4}	4.3±0.75

accuracy compared with the ACO algorithm. The standard deviation of the iteration numbers calculated by the HAPO algorithm is smaller than that by the ACO algorithm.

Multi-parameter retrieval

In order to illustrate the performance of the ACO algorithms, the thermal conductivity, λ, absorption coefficient, κ_a, and scattering coefficient, κ_s, are retrieved simultaneously. In the model depicted in the chapter *Forward model*, the boundary conditions are set as the same as that in the section *Single parameter retrieval*. The three parameters are retrieved simultaneously by measuring the temperature and radiative heat flux on the borders when the true values are assumed: $\lambda^* = 20$ Wm/K, $\kappa_a^* = 0.5\ \mathrm{m}^{-1}$, and $\kappa_s^* = 4.5\ \mathrm{m}^{-1}$, where the measured values are obtained by using the FVM approximation with $N_x = 5000$ and $N_\theta = 100$.

To further illustrate the performance of the ACO algorithms, random errors are considered. Measured values with random errors are obtained by adding normal distributed errors to the actual measured values:

$$M_l = M_{\mathrm{exa},\,l} + \mathrm{rand_n}\sigma_l\,, \qquad (l = 1, 2, \cdots, N_\mathrm{m}) \tag{23}$$

where M_l is the actual measured value in the l^{th} position, $M_{\mathrm{exa},\,l}$ – the exact measured value in the l^{th} position, $\mathrm{rand_n}$ is a normal distributed random variable with zero mean and unit standard deviation. The standard deviation of measured value σ_l, for a measurement error of $\gamma\%$ at 99% confidence, is determined:

$$\sigma_l = \frac{z^*_{l,\mathrm{exa}}\ \gamma\%}{2.576} \tag{24}$$

where 2.576 arises from the fact that 99% of a normal distributed population is contained within ±2.576 standard deviation of the mean value.

Measured values with $\gamma\%$ noise are used to estimate the thermal conductivity, absorption coefficient, and scattering coefficient, where the measurement errors $\gamma\%$ are set as 1, 2, and 5%, respectively. Taking the FVM approximation with $N_x = 300$ and $N_\theta = 50$ as the forward model in the inversion, the inversion parameters are retrieved by using the two ACO algorithms. The system data and control parameters and the stop criterion parameters are set as the same as that in the section *Single parameter retrieval*. The ACO algorithms are both implemented for 100 times to reduce the randomness. The retrieval results are shown in tab. 4. The initial search space of the inversion parameters are set as $\lambda \in [0, 100]$, $\kappa_a \in [0, 10]$, and $\kappa_s \in [0, 10]$, respectively.

As shown in tab. 4, compared with the ACO algorithm, the efficiency of the HAPO algorithm is much higher, although the accuracy of the HAPO algorithm is slightly decreased. For average retrieval results, the largest relative error of these two algorithms is less than 4.6% even with a measurement error of 5%, which demonstrates the robustness of the PDF-based ACO algorithms is high. It is noteworthy that the standard deviation of the iteration numbers seems decreasing with the increase in measurement errors. That is because we set the maximum number of iterations as $N_\mathrm{g} = 1000$. This does not mean that the stability of the ACO algorithm increases with the increasing of measurement errors. We can also see from tab. 4 that the standard deviation of the retrieval results and the iteration numbers increase with the increasing of the measurement errors. Averaging multiple retrieved results can effectively reduce the retrieval errors of the stochastic optimization algorithms, especially when retrieving multiple parameters by few measurement values.

Table 4. The influence of measurement errors on the retrieval results of the three parameters

Algorithm	γ%	Iteration, t	λ [$Wm^{-1}K^{-1}$]	κ_a [m^{-1}]	κ_s [m^{-1}]
ACO	0	510±154	19.96±0.14	0.505±0.017	4.491±0.213
	1	983±80	19.97±0.90	0.513±0.059	4.455±0.218
	2	1000±0	20.15±1.50	0.516±0.064	4.450±0.222
	5	1000±0	19.70±2.89	0.520±0.126	4.364±0.238
HAPO	0	77±21	19.92±0.30	0.510±0.035	4.483±0.213
	1	145±56	19.87±1.15	0.518±0.083	4.493±0.230
	2	311±227	19.93±1.37	0.522±0.097	4.350±0.259
	5	785±286	19.81±2.80	0.523±0.105	4.434±0.272

Conclusions

In the present study, a PDF-based ACO algorithm for continuous domain has been applied to the inverse problems of coupled radiative and conductive heat transfer. By bringing in the idea of the PSO algorithm, the HAPO algorithm is developed on the basis of the ACO algorithm. The thermal conductivity, absorption coefficient, and scattering coefficient can be retrieved simultaneously by four steady-state measured signals on the borders. The HAPO algorithm is proved to be more effective and robust via several test cases. By increasing the number of the inversion parameters, the accuracies of the retrieval results are decreasing correspondingly. However, the errors of the average multiple retrieval results are still in the tolerant limit. It is an effective way to reduce the retrieval error for measured values with normal distributed errors especially for retrieving multiple parameters by few measured values.

Acknowledgment

The supports of this work by the Foundation for Innovative Research Groups of the National Natural Science Foundation of China (No. 51421063), the Major National Scientific Instruments and Equipment Development Special Foundation of China (No. 51327803), and the National Natural Science Foundation of China (No. 51576053) are gratefully acknowledged.

Nomenclature

c_1, c_2 – acceleration coefficient, [–]
F – objective function value, [–]
$f_{\eta_{i,j}}$ – probability density function, [–]
h – convective coefficient, [$Wm^{-2}K^{-1}$]
high – high limit of the search space, [–]
I – radiative intensity, [$Wm^{-2}sr^{-1}$]
k – the control parameter of colony size
L – length of the media, [m]
low – low limit of the search space, [–]
M – measured value, [–]
N – number, [–]
$\vec{n}$ – outward normal direction, [–]
$P_{i,j}$ – probability, [–]
P_1, P_g – local and global best position, [–]
q – heat flux, [Wm^{-2}]
$rand_n$ – normal random number, [–]
$rand_u$ – uniform random number, [–]
s – distance along a certain direction, [m]
T_{f1} – temperature of the left ambient, [K]
T_{f2} – temperature of the right ambient, [K]
t – iteration, [–]
v_i – particle velocity, [–]
w_{τ_j} – weight factor, [–]
x_i – location, [–]

Greek symbols

α – weight control parameter, [–]
β – convergence control parameter, [–]
γ – measurement error, [%]
ε – emissivity, [–]

ε_d, ε_o – tolerance, [–]
θ – angle with x direction
κ_a, κ_e, κ_s – radiative parameters, [m^{-1}]
λ – thermal conductivity, [$Wm^{-1}K^{-1}$]
μ_i – mean best retrieval value, [–]
$\mu_{i,j}$ – retrieval value, [–]
ρ – speed control parameter, [–]
σ – Stefan-Boltzmann constant, [$Wm^{-2}K^{-4}$]
$\sigma_{i,j}$ – standard deviation, [–]
Φ – scattering phase function, [–]
Ω – solid angle, [sr]
$\vec{\Omega}$, $\vec{\Omega}'$ – incoming and outgoing direction, [–]
ξ – acceleration control parameter, [–]

Superscripts

+ – positive direction
– – negative direction
r – radiative

Subscripts

a – ant
b – black body
d – dominant ant ranks
exa – exact
f – ambient
g – generation
i – inverse index
j – rank index
l – measurement index
obj – objective function
s – success
t – total
w – wall
x – space mesh
θ – angle mesh
* – true value

References

[1] Ruan, L. M., *et al.*, Development of a Finite Element Model for Coupled Radiative and Conductive Heat Transfer in Participating Media, *Journal of Quantitative Spectroscopy and Radiative Transfer*, *102* (2006), 2, pp. 190-202
[2] Yi, H. L., *et al.*, Coupled Radiation and Solidification Heat Transfer Inside a Graded Index Medium by Finite Element Method, *International Journal of Heat and Mass Transfer*, *54* (2011), 13-14, pp. 3090-3095
[3] Lari, K., Gandjalikhan, N. A. S., Modeling of the Conjugate Radiation and Conduction Problem in a 3D Complex Multi-Burner Furnace, *Thermal Science*, *16* (2012), 4, pp. 1187-1200
[4] Zhang, Y., *et al.*, Natural Element Method Analysis for Coupled Radiative and Conductive Heat Transfer in Semitransparent Medium with Irregular Geometries, *International Journal of Thermal Sciences*, *76* (2014), Feb., pp. 30-42
[5] Talukdar, P., *et al.*, Modelling of Conduction-Radiation in a Porous Medium with Blocked-off Region Approach, *International Journal of Thermal Sciences*, *72* (2013), Oct., pp. 102-114
[6] Mishra, S. C., Sahai, H., Analysis of Non-Fourier Conduction and Radiation in a Cylindrical Medium Using Lattice Boltzmann Method and Finite Volume Method, *International Journal of Heat and Mass Transfer*, *61* (2013), June, pp. 41-55
[7] Zhang, B., *et al.*, Application of Homogenous Continuous Ant Colony Optimization Algorithm to Inverse Problem of One-Dimensional Coupled Radiation and Conduction Heat Transfer, *International Journal of Heat and Mass Transfer*, *66* (2013), Nov., pp. 507-516
[8] Chopade, R. P., *et al.*, Simultaneous Retrieval of Parameters in a Transient Conduction-Radiation Problem Using a Differential Evolution Algorithm, *Numerical Heat Transfer, Part A: Applications*, *63* (2013), 5, pp. 373-395
[9] Chopade, R. P., *et al.*, Application of a Particle Swarm Algorithm for Parameter Retrieval in a Transient Conduction-Radiation Problem, *Numerical Heat Transfer, Part A: Applications*, *59* (2011), 9, pp. 672-692
[10] Das, R., *et al.*, An Inverse Analysis for Parameter Estimation Applied to a Non-Fourier Conduction–Radiation Problem, *Heat Transfer Engineering*, *32* (2011), 6, pp. 455-466
[11] Zhang, B., *et al.*, Inverse Transient Radiation Analysis in One-Dimensional Participating Slab Using Improved Ant Colony Optimization Algorithms, *Journal of Quantitative Spectroscopy and Radiative Transfer*, *133* (2014), Jan., pp. 351-363
[12] Qi, H., *et al.*, Application of Multi-Phase Particle Swarm Optimization Technique to Inverse Radiation Problem, *Journal of Quantitative Spectroscopy and Radiative Transfer*, *109* (2008), 3, pp. 476-493
[13] Colorni, A., *et al.*, Distributed Optimization by Ant Colonies, *Proceedings*, 1st European Conference on Artificial Life, Paris, 1991, pp. 134-142
[14] Dorigo, M., *et al.*, Ant Algorithms for Discrete Optimization, *Artificial Life*, *5* (1999), 2, pp. 137-172
[15] Qi, H., *et al.*, Retrieval of Spherical Particle Size Distribution Using Ant Colony Optimization Algorithm, *Chinese Optics Letters*, *11* (2013), 11, pp. 112901-1-5

[16] Socha, K., ACO for Continuous and Mixed-Variable Optimization, *Proceedings*, 4th International Workshop on Ant Colony Optimization and Swarm Intelligence, Brussels, 2004, pp. 25-36
[17] Fernandez-Vargas, J. A., *et al.*, An Improved Ant Colony Optimization Method and its Application for the Thermodynamic Modeling of Phase Equilibrium, *Fluid Phase Equilibria*, *353* (2013), Sep., pp. 121-131
[18] Huang, C. L., *et al.*, Hybridization Strategies for Continuous Ant Colony Optimization and Particle Swarm Optimization Applied to Data Clustering, *Applied Soft Computing*, *13* (2013), 9, pp. 3864-3872
[19] Li, X., *et al.*, Rolling Element Bearing Fault Detection Using Support Vector Machine with Improved Ant Colony Optimization, *Measurement*, *46* (2013), 8, pp. 2726-2734
[20] Qi, H., *et al.*, Inverse Radiation Analysis of a One-Dimensional Participating Slab by Stochastic Particle Swarm Optimizer Algorithm, *International Journal of Thermal Sciences*, *46* (2007), 7, pp. 649-661
[21] Qi, H., *et al.*, Application of Multi-Phase Particle Swarm Optimization Technique to Retrieve the Particle Size Distribution, *Chinese Optics Letters*, *6* (2008), 5, pp. 346-349
[22] Qi, H., *et al.*, Inverse Transient Radiation Analysis in One-Dimensional Non-Homogeneous Participating Slabs Using Particle Swarm Optimization Algorithms, *Journal of Quantitative Spectroscopy and Radiative Transfer*, *112* (2011), 15, pp. 2507-2519
[23] Sun, Y. P., *et al.*, Estimating Soot Volume Fraction and Temperature in Flames Using Stochastic Particle Swarm Optimization Algorithm, *International Journal of Heat and Mass Transfer*, *54* (2011), 1-3, pp. 217-224
[24] Wang, D. L., *et al.*, Retrieve Properties of Participating Media by Different Spans of Radiative Signals Using the SPSO Algorithm, *Inverse Problems in Science and Engineering*, *21* (2013), 5, pp. 888-915
[25] Modest, M. F., *Radiative Heat Transfer*, McGraw-Hill, New York, USA, 2003

Paper submitted: November 11, 2013
Paper revised: January 24, 2014
Paper accepted: February 25, 2014